Conductivity and Transparency of ZnO/SnO_2-Cosubstituted In_2O_3

G. B. Palmer and K. R. Poeppelmeier*

Department of Chemistry and Materials Research Center, Northwestern University, Evanston, Illinois 60208

T. O. Mason

Department of Materials Science and Materials Research Center, Northwestern University, Evanston, Illinois 60208

Received June 4, 1997[⊗]

In_2O_3 exhibits a dramatic increase in solubility of SnO_2 and ZnO when they are cosubstituted into In_2O_3. The resultant material, $In_{2-2x}Sn_xZn_xO_{3-\delta}$ with $x = 0-0.4$, displays the same order of magnitude conductivity and transparency compared with bulk ITO (tin-doped indium oxide). Rapid quenching of $In_{2-2x}Sn_xZn_xO_{3-\delta}$ raises the conductivity and widens the optical bandgap while lowering the optical transmission.

Introduction

ITO (tin-doped indium oxide) is a TCO (transparent conducting oxide), widely used for flat-panel display electrodes. ITO has a typical conductivity of $(1-5) \times 10^3$ S/cm and a transparency of 85−90% in thin films.[1] Although ITO meets the needs of current devices, research is ongoing to develop new TCOs with improved physical properties.

In addition to ITO, which has been reviewed,[2] a number of promising TCOs consisting of various oxide combinations of In, Sn, and Zn have been reported. Wang et al.[3] reported a conductivity of 1100 S/cm in sputtered ZnO films with 5 cation % In doping. Minami et al.[4] reported a conductivity of 2900 S/cm in sputtered $Zn_2In_2O_5$ films. Phillips et al.[5] reported a conductivity of 2500 S/cm for a pulsed-laser deposited film with an approximate composition of $ZnIn_{1.7}Sn_{0.3}O_{4.15-\delta}$ but were unable to determine the chemical phase. Moriga et al.[6] measured the conductivity and transparency of bulk samples of reduced and unreduced $Zn_kIn_2O_{3+k-\delta}$ for $k = 3, 4, 5, 7, 11$. They observed higher conductivity and lower transparency at low k numbers. The highest conductivity reported was 270 S/cm for bulk, reduced $Zn_3In_2O_{6-\delta}$. Palmer et al.[7] studied bulk, reduced Zn_2SnO_4 and showed that In substitution improved conductivity.

Although nonequilibrium conditions can exist in thin films, knowledge of equilibrium phase relationships and bulk physical properties of stable phases can assist interpretation of known film materials and direct new materials film synthesis. Wen et al.[8] studied bulk powders of In_2O_3 to determine the optimum single cation dopant. However, there has been little study of combinations of substituted cations in In_2O_3. In this article, we present the phase relations and physical properties of SnO_2/ZnO-cosubstituted In_2O_3: $In_{2-2x}Sn_xZn_xO_{3-\delta}$, $x = 0-0.4$.

Table 1. Sample Compositions and Preparation

				1100 °C		1250 °C	
sample	% $InO_{1.5}$	% SnO_2	% ZnO	sintering time (days)	(% mass loss)	sintering time (days)	(% mass loss)
146	100	0	0	5.0	0.5	7.0	0.6
149	96	4	0	5.0	0.3	7.0	3.2
161	95	2.5	2.5	6.0	0.4	4.2	0.9
131	90	5	5	2.7	0.7	11.0	1.4
160	85	7.5	7.5	6.0	0.5	4.2	1.0
159	80	10	10	6.0	0.4	4.2	1.3
158	75	12.5	12.5	6.0	0.4	4.2	0.8
127	70	15	15	2.6	0.4	3.0	2.8
154	60	20	20	4.0	0.2	4.2	0.4
117	50	25	25	5.0		4.7	0.4
102	50	25	25	5.0	0.4	6.8	
153	97.8	2.2	0	5.9	0	4.0	1.6
147	0	100	0	5.0	0.1	7.0	0.4
148	0	0	100	5.0	0.2	7.0	9.8

Experimental Section

Synthesis. As shown in Table 1, most compositions consisted of equimolar amounts of SnO_2 and ZnO mixed with In_2O_3. For reference purposes, pure samples of In_2O_3, SnO_2, and ZnO were prepared as well as a 4 cation % Sn ITO sample and a 2.2 cation % Zn−97.8 cation % In oxide sample. Powders were prepared from 99.99% In_2O_3, 99.9% SnO_2, and 99.99% ZnO (cation basis, Aldrich Chemical Co.). 2 g samples were ground together under acetone with an agate mortar and pestle. 1.27 cm (0.5 in.) pellets were uniaxially pressed in a steel die at 51.7 MPa (Carver 3392 Laboratory Press). Sample pellets were fired in alumina crucibles. The pellets were buried in their constituent powders to minimize reaction with the alumina crucibles or evaporation of the metal oxides.

[⊗] Abstract published in *Advance ACS Abstracts,* November 1, 1997.

(1) Lyman, N. R. *Proc. Symp. Electrochrom. Mater., Electrochem. Soc.* **1990**, *90−92*, 201−231.
(2) Hamberg, I.; Granqvist, C. *J. Appl. Phys.* **1986**, *60*, R123.
(3) Wang, R.; Sleight, A.; Platzer, R.; Gardner, J. A. *J. Mater. Res.* **1996**, *11*, 1659.
(4) Minami, T.; Kakumu, T.; Takata, S. *J. Vac. Sci. Technol. A* **1996**, *14*, 1704.
(5) Phillips, J. M.; Cava, R. J.; Thomas, G. A.; Carter, S. A.; Kwo, J.; Siegrist, T.; Krajewski, J.; Marshall, J.; Peck, W.; Rapkine, D. *Appl. Phys. Lett.* **1995**, *67*, 2246.
(6) Moriga, T.; Edwards, D.; Mason, T.; Palmer, G.; Poeppelmeier, K.; Schindler, J.; Kannewurf, C.; Nakabayashi, I. *J. Am. Ceram. Soc.*, in press.
(7) Palmer, G. B.; Poeppelmeier, K. R.; Mason, T. O. *J. Solid State Chem.*, in press.
(8) Wen, S. J.; Campet, G.; Portier, J.; Couturier, G.; Goodenough, J. B. *Mater. Sci. Eng.* **1992**, *B14*, 115.

S0897-4756(97)00403-1 CCC: $14.00

Samples were initially heated at 1100 °C. The samples were then removed, reground, and repelletized, prior to a 1250 °C heating. Sintering times and pellet mass losses are shown in Table 1.

Two cooling methods were used. The "air-quenched" sample crucibles were removed from the at-temperature furnace and cooled in ambient air, resulting in room-temperature pellets in about 20 min. The "copper-quenched" samples were removed from the at-temperature furnace and placed immediately on a copper plate heat sink. The glowing pellets and powders were moved around on the copper plate to accelerate cooling, which was complete within a few seconds. Visual inspection of the copper plate and sample pellets showed no copper melting or copper reaction with the pellets.

X-ray Crystallography. Powder X-ray diffraction was used to determine phase composition after both firings (Rigaku). Copper Kα radiation was used at 40 kV and 20 mA. LiF (JCPDS Card No. 4-857, Copper Kα_1) was used as an internal X-ray standard. The average shift of the observed LiF peaks was used to make an off-axis correction (2θ shift) to the sample peaks. The X-ray peaks were fitted using Xrayfit.[9] Lattice constants were calculated with a least-squares averaging program, POLSQ,[10] using the weighted average Kα wavelength, 1.5418 Å.

Electronic Measurements. Room-temperature electrical conductivities of as-fired pellets were measured with a spring-loaded linear four-probe apparatus. Excitation currents ranged from 1 to 50 mA (Model 225, Keithly Current Source). Voltages were measured with a voltmeter (Model 197, Keithly). The conductivity was calculated as

$$\sigma = \frac{1}{\rho} = \frac{1}{\frac{V}{I} w C\left(\frac{d}{s}\right) F\left(\frac{w}{s}\right)}$$

where σ is conductivity, ρ is resistivity, V is measured voltage, I is excitation current, w is width, d is diameter, s is electrode spacing, and $C(d/s)$ and $F(w/s)$ are correction factors for sample geometry and finite thickness, respectively.[11] To ensure meaningful comparisons, each conductivity was normalized by the percent theoretical density of the sintered sample.

Optical Measurements. The diffuse reflectance of as-fired pellets was measured from 190 to 800 nm using a double beam spectrophotometer with integrating sphere (Cary 1E with Cary 1/3 attachment, Varian). A pressed PTFE powder compact (Varian Part No. 04-101439-00) was used as a high transmission reference. A blackened sample mask was used to mount pellet samples. A background scan with the sample mask was performed and subtracted from all spectra. To limit specular reflectance, as-fired pellets were used with no surface polishing. After diffuse reflectance, the samples were cut and the pellet cross sections compared visually to the exterior surfaces. There were no discernible color differences.

Results and Discussion

Appearance and Morphology. After firing, all samples were sintered into semihard pellets. Theoretical densities were calculated from observed lattice parameters and starting mixture stoichiometry. Pellet densities were calculated directly from pellet mass and dimensions. Densities averaged 50% of theoretical and are shown in Table 2. Pellets were sturdy enough to be handled and cut by a diamond saw blade. However, they shattered easily when hand-cutting with a razor blade was attempted.

Pellet colors were summarized in Table 2. All samples were visually homogeneous except sample 153 (2.2 cation % Zn/97.8 cation % In). The pure In_2O_3 sample (number 146) was bright yellow. All cosubstituted samples and the ITO reference sample were grayish green. The ITO pellet and the (copper-quenched) 90 cation % In pellet were the darkest samples. The air-quenched pellets 161, 160, 159, 158, 154 displayed increased darkening as the amount of cosubstitution increased.

Table 2. Sample Quenching, Colors, and Densities

sample	quenching method	color	fraction of theoretical density
146	copper	yellow	0.52
149	copper	dark gray-green	0.51
161	air	gray-green	0.51
131	copper	dark gray-green	0.48
160	air	gray-green	0.53
159	air	gray-green	0.47
158	air	gray-green	0.51
127	copper	gray-green	0.41
154	air	gray-green	0.44
117	copper	green	0.59
102	air		
153	copper	yellow w/green spots	0.51
147	copper	white	
148	copper	jade green	0.65

Crystal Structure and Phase Equilibria. In_2O_3 (JCPDS Card No. 6-416) crystallizes in the C-type rare-earth (bixbyite) structure.[12] The unit cell is body-centered cubic (space group $Ia\bar{3}$) with lattice parameter, $a = 10.117(1)$ Å. The structure can be derived from the fluorite structure by ordered removal of one-quarter of the anions. All In^{3+} cations are 6-coordinate and all O^{2-} anions are 4-coordinate. In^{3+} cations are located on two crystallographically distinct sites: one with In−O bond lengths = 2.18 Å, and one with pairs of In−O bond lengths = 2.13, 2.19, 2.23 Å.

All samples were phase-pure by X-ray diffraction, except the two 50 cation % In samples which exceeded the cosubstitution limit of ZnO and SnO_2 in In_2O_3. All cosubstituted samples showed the bixbyite structure reflections without new peaks or systematic absences and the relative peak intensities were similar throughout the solubility range. On the basis of this evidence, the cubic bixbyite structure was shown to be preserved without noticeable distortion other than lattice parameter contractions.

Figure 1 shows the change in cubic lattice parameter, a, with cosubstitution in $In_{2-2x}Sn_xZn_xO_{3-\delta}$. The inset graphic shows the 721 peak of $x = 0$ and $x = 0.4$ samples. As x increases, the X-ray reflections shift to higher values, indicating that the unit cell gets smaller. The lattice parameter shift follows Vegard's rule, as shown by the linear relationship, with correlation coefficient, $r = 0.98$. The smaller lattice parameter of cosubstituted In_2O_3 is consistent with the ionic radii of the cosubstituted species. Both Zn^{2+} (0.740 Å) and Sn^{4+} (0.690) have smaller 6-coordinate ionic radii than In^{3+} (0.800 Å).[13] Figure 1 indicates a cosubstitution limit at roughly 60 cation % In.

In contrast to $In_{2-2x}Sn_xZn_xO_{3-\delta}$, the binary systems $In_2O_3-SnO_2$ (ITO) and In_2O_3-ZnO show small solid solubilities. Furthermore, the $In_2O_3-SnO_2$ solid solution exhibits large deviations from Vegard's rule. For

(9) Georgopoulos, P. XRAYFIT, Fortran program, Northwestern University, Evanston, IL, 1993.
(10) Keszler, D.; Cahen D.; Ibers, J. POLSQ, Fortran program, Northwestern University, Evanston, IL, 1984.
(11) Smits, F. M. *Bell Syst. Techn. J.* **1958**, *37*, 711.
(12) Marezio, M. *Acta Crystallogr.* **1966**, *20*, 723.
(13) Shannon, R. D. *Acta Crystallogr.* **1976**, *A32*, 751.

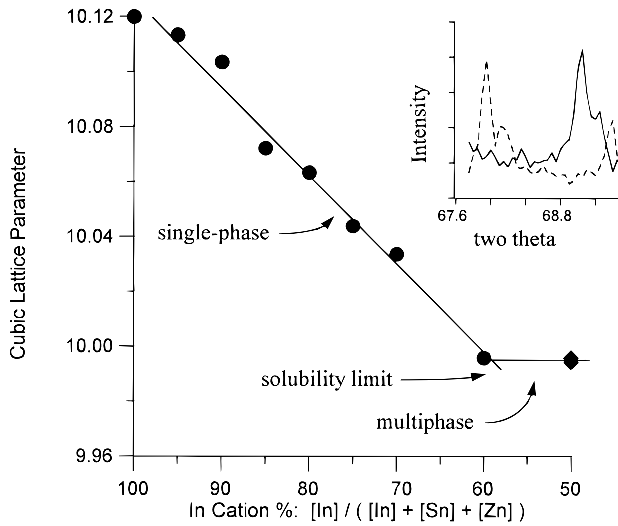

Figure 1. Lattice parameter versus cation % In. The sloping region is single phase. The horizontal line is three phase. The inset powder pattern shows the pronounced two theta shift of the 721 peak between In_2O_3 (dashed line) and $In_{1.2}Sn_{0.4}Zn_{0.4}O_3$ (solid line).

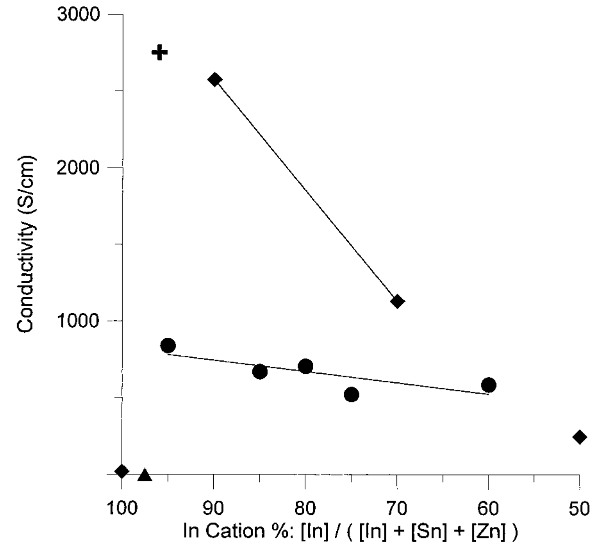

Figure 2. Conductivity versus cation % In. Samples shown are (◆) cosubstituted copper-quenched including In_2O_3, (●) air-quenched cosubstituted, (+) 4 cation % Sn ITO, (▲) 97.8 cation % In/2.2 cation % Zn oxide.

ITO, Enoki et al.[14] showed 6.6 cation % solid solubility of SnO_2 in In_2O_3 at 1300 °C. Frank et al. found a 6 ± 2 cation % solubility of SnO_2 in In_2O_3 in powders[15] at 1000 °C and a 7 ± 2% solubility limit in single crystals grown from molten metals[16] at 600 °C. In ITO films,[17] Frank and Köstlin showed that the lattice parameter had a small decrease over the first 2 cation % of Sn substitution, followed by a large increase with additional Sn doping. Consistent with earlier work, this study showed nonideal (based on dopant ionic radii) ITO lattice size effects. Specifically, a 4 cation % Sn (ITO) sample had a lattice parameter of 10.125 Å as compared to an observed In_2O_3 lattice parameter of 10.120 Å.

No noticeable solid solubility of ZnO into In_2O_3 has been reported. Moriga et al.[18] determined phase relations in the $ZnO-In_2O_3$ pseudobinary and observed a two-phase assemblage of In_2O_3 and $Zn_4In_2O_7$, produced at 1250 °C from an 80 cation % In sample. They observed equal lattice parameters of pure In_2O_3 and In_2O_3 in equilibrium with $Zn_4In_2O_7$ and therefore concluded that there was minimal solubility of ZnO in In_2O_3. Nakamura et al.[19] prepared a two-phase sample of In_2O_3 and $Zn_3In_2O_6$ at 1350 °C from an 80 cation % In starting mixture and also observed no change in the In_2O_3 lattice constant. To confirm these results, especially given the nonideal lattice shifts observed in ITO, a 2.2 cation % ZnO−97.8 cation % In_2O_3 sample was prepared for this study. The as-fired pellet had small spots of green in an otherwise yellow pellet. On the basis of visual comparison to pellets from the Moriga study,[6] it appears that the sample was In_2O_3 (yellow) with small regions of $Zn_4In_2O_7$ or $Zn_3In_2O_6$ (green). No X-ray evidence for a Zn−In oxide compound was seen, presumably because of the small amount of the Zn−In−O phase and its relatively weak reflections.[20] The observed In_2O_3 lattice constant was the same as that of pure In_2O_3. On the basis of the visual appearance, the sample was determined to be two-phase. From this direct evidence, ZnO solubility is less than 2.2 cation % at 1250 °C.

The different phase behaviors of cosubstituted In_2O_3 as compared to In_2O_3 (SnO_2) and In_2O_3 (ZnO) reflect the ease of *iso*valent substitution versus the difficulty of *alio*valent substitution. In ITO, Sn^{4+} cations are aliovalently incorporated onto In^{3+} sites. This disrupts local electroneutrality, limits solubility and causes nonideal Vegard's rule behavior. Because of the aliovalent substitution, ITO shows a strong tendency for incorporation of compensating O^{2-}, which reduces the Sn doping efficiency.[17] In $In_{2-2x}Sn_xZn_xO_{3-\delta}$, one Sn^{4+} and one Zn^{2+} are introduced for every two In^{3+} removed. The overall effect is isovalent substitution which allows extensive solid solubility.

Electronic Properties. Figure 2 shows the room-temperature conductivity of samples versus cation % In along the cosubstitution regime. In addition to the phase-pure cosubstituted samples, a 4 cation % Sn ITO sample, a pure In_2O_3 sample, and mixed-phase samples with ZnO doping and excess cosubstitution are compared. Pure In_2O_3 is a relatively poor conductor (19.8 S/cm) compared to any of the Sn-containing compounds. The multiphase 2.2 cation % ZnO/97.8 cation % In_2O_3 pellet (containing In_2O_3 saturated with ZnO) showed conductivity 2 orders of magnitude lower than pure In_2O_3 (0.149 S/cm). The 4 cation % Sn-doped ITO sample showed the highest conductivity overall. However, the cosubstituted pellet at 90 cation % In had similar overall conductivity (2575 versus 2752 S/cm for ITO). Moreover, all cosubstituted samples showed conductivities greater than 500 S/cm.

(14) Enoki, H.; Echigoya, J.; Suto, H. *J. Mater. Sci.* **1991**, *26*, 4110.
(15) Frank, G.; Köstlin, H. *Phys. Status Solidi* **1979**, *52*, 231.
(16) Frank, G.; Brock, L.; Bausen, H. *J. Cryst. Growth* **1976**, *36*, 179.
(17) Frank, G.; Köstlin, H. *Appl. Phys. A* **1982**, *27*, 197.
(18) Moriga, T.; Edwards, D.; Mason, T.; Palmer, G.; Poeppelmeier, K.; Schindler, J.; Kannewurf, C.; Nakabayashi, I. *J. Am. Ceram. Soc.*, submitted.
(19) Nakamura, M.; Kimizuka, N.; Mohri, T. *J. Solid State Chem.* **1990**, *86*, 16.

(20) Analysis of several similarly prepared X-ray samples of phase-pure samples, showed that the strongest peaks of phase-pure samples of $Zn_4In_2O_7$ or $Zn_3In_20_6$ were always 25−50% of the intensity of the strongest (222) peak of In_2O_3. This is reasonable considering the higher symmetry of In_2O_3.

If the cosubstitution conductivity data (leaving out the pure In_2O_3 sample) are separated into sets based on quenching method, two trends appear. First, conductivity for both data sets drops as the amount of cosubstitution increases. This decline in conductivity is more pronounced for the copper-quenched samples than the air-quenched samples. Second, the copper-quenched samples appear to have larger relative conductivities than the air-quenched samples.

The higher conductivity of copper-quenched samples is evidence of the reducing effects of high temperature. Examining the equation for oxygen vacancy donor formation:

$$O_O^x \rightarrow {}^1/_2O_2(g) + V_O^{\bullet\bullet} = 2e'$$

Because the enthalpy change of reaction, ΔH_{rxn}, is positive,[21] higher temperatures lead to a larger equilibrium concentration of oxygen vacancies. Presumably, rapid quenching preserves some of the high-temperature oxygen vacancies, while slow cooling allows filling of vacancies. These vacancies contribute to conductivity since reoxidation at room temperature is relatively slow.[22]

It might be expected that the Zn^{2+}/Sn^{4+} cosubstitution should produce donor−acceptor pairs in the material and not give any overall carriers. However, the significantly higher conductivities of cosubstituted samples compared to In_2O_3 indicate some form of carrier production in these materials.

It is possible that the cosubstituted samples have a slight (but electronically significant) imbalance of Sn^{4+} compared to Zn^{2+}. The excess Sn^{4+} would then create net donors. This explanation is supported by the discernible weight loss of the pellets during firing as shown in Table 1, especially for the pure ZnO sample. Preferential ZnO loss would result in a Sn^{4+}/Zn^{2+} ratio greater than one in the cosubstituted samples. The original rationale for the initial 1100 °C heating was to incorporate as much ZnO as possible into the compound prior to vaporization. On the basis of prior experience, in zinc containing compounds, the rate of Zn loss can be significantly less compared to pure ZnO. However, it is still possible that preferential evaporation of ZnO may have occurred during or after formation of the cosubstituted samples, resulting in samples slightly richer in Sn^{4+} than Zn^{2+}.

Presumably, then, the improved conductivity of copper-quenched samples would be from removal of excess (compensating) oxygen attracted by the excess Sn^{4+} cations. The rapid quench would be analagous to the postdeposition reductions often performed on ITO films to enhance their conductivities.

Another explanation of the high conductivity of cosubstituted samples is the formation of oxygen vacancy donors. In this case, Sn^{4+} and Zn^{2+} would be present in equal amounts, as determined by the starting mixture stoichiometries. However the presence of Zn^{2+} cations in the bixbyite structure might stabilize formation of oxygen vacancies. It is also possible that some combination of enhanced oxygen vacancy formation and excess Sn^{4+} are responsible for the observed conductivities.

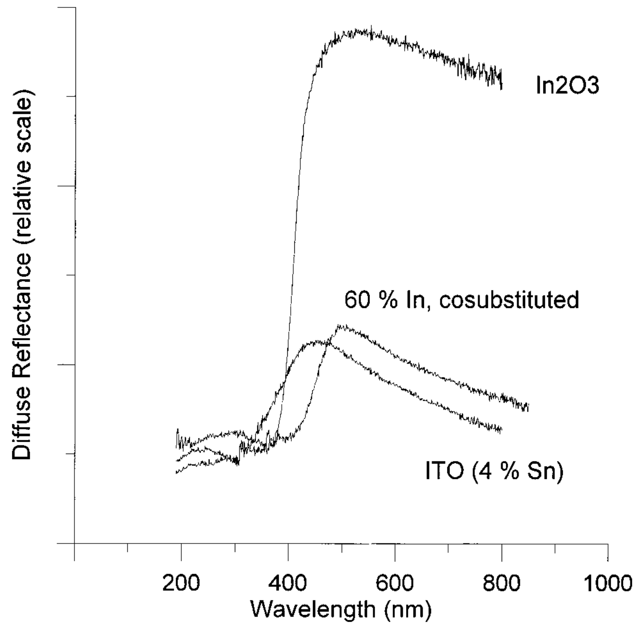

Figure 3. Diffuse reflectance spectra of In_2O_3, ITO, and cosubstituted In_2O_3.

Optical Properties. Figure 3 shows diffuse reflectometry spectra for pure In_2O_3, ITO, and a representative cosubstituted sample. Diffuse reflectometry is analogous to transmission and allows relative comparisons of transmission for bulk samples.[23] The optical bandgap and peak visible transmission of the samples were analyzed and plotted. The optical bandgap was assumed to be roughly equal to the transmission edge onset as defined by the intersection of lines constructed from the low transmission UV region and the slope approaching the transmission region. All spectra had peak transmissions close to 500 nm.

Figure 4 shows the optical bandgaps versus percent In and conductivity. The ITO pellet has a wider bandgap than the pure In_2O_3 pellet (Moss−Burstein[24] shift). Of the cosubstituted samples, only the 90 cation % In sample shows a wider bandgap than In_2O_3. Two trends are evident. Increased conductivity correlates with higher bandgaps and increased cosubstitution correlates with lower bandgaps.

Burstein[24] showed that in degenerate semiconductors with curved bands, filling of states caused a widening of the direct optical bandgap (see Figure 6). Granqvist et al. showed that in ZnO,[25] SnO_2,[26] and ITO[27] the calculated Moss−Burstein bandgap widening was partially offset by bandgap narrowing from many-body interactions. However, they still noted larger overall bandgaps for materials with higher carrier concentrations. A third factor is required to explain the bandgaps observed in $In_{2-2x}Sn_xZn_xO_{3-\delta}$. We propose that donor−acceptor pairs formed from Zn^{2+} and Sn^{4+} cause bandgap narrowing in the cosubstituted material.

This explanation is supported by the observed dependence of bandgap shift on conductivity and cosubstitu-

(21) De Wit, J. H. W. *J. Solid State Chem.* **1975**, *13*, 192.
(22) Samples stored in ambient air had unchanged conductivity after 2 months.
(23) Hecht, H. In *Modern Aspects of Reflectance Spectroscopy*; Wendlandt, W., Ed.; Plenum Press: New York, 1968; pp 1−22.
(24) Burstein, E. *Phys. Rev.* **1954**, *93*, 632.
(25) Jin, Z.; Hamberg, I.; Granqvist, C. *J. Appl. Phys.* **1988**, *64*, 5117.
(26) Sterjna, B.; Granqvist, C. *Thin Solid Films.* **1990**, *193/194*, 704.
(27) Hamberg, I.; Granqvist, C. *J. Appl. Phys.* **1986**, *60*, R123.

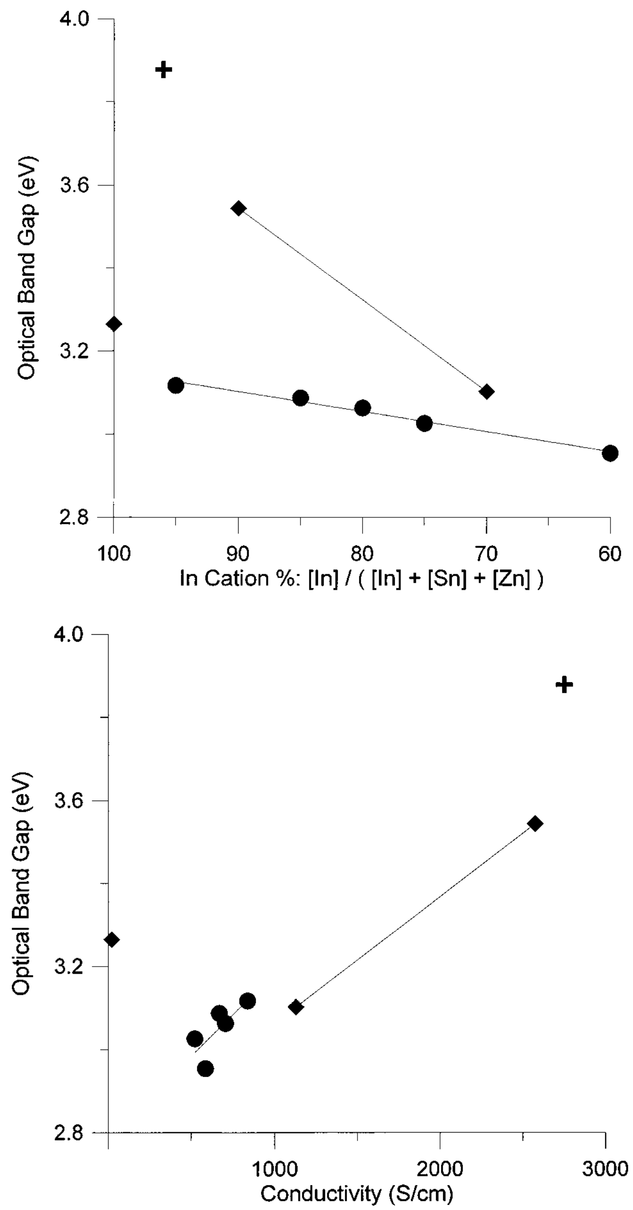

Figure 4. Optical bandgap versus cation % In (a, top) and versus conductivity (b, bottom). Samples shown are (◆) cosubstituted copper-quenched including pure In$_2$O$_3$, (●) air-quenched cosubstituted, (+) 4 cation % Sn ITO.

tion extent (Figure 4). All cosubstituted samples, except the highest conductivity sample, showed overall bandgap narrowing even though conductivities were an order of magnitude higher than in pure In$_2$O$_3$. In addition, the high conductivity (90 cation % In) cosubstituted sample had a comparable conductivity to the ITO pellet (2575 versus 2752 S/cm), but the ITO pellet had a wider bandgap (3.87 versus 3.54 eV). Moreover, comparison of the copper-quenched 70 cation % In and air-quenched 95 cation % In samples showed that the higher conductivity, more cosubstituted sample had a slightly narrower bandgap than the lower conductivity, less cosubstituted sample. For these comparisons conductivity was used as an indicator of carrier concentration. This is reasonable, because increased cosubstitution should create more electronic scattering centers and lower electronic mobility. Hence the conductivities of more cosubstituted samples may actually underestimate carrier concentrations.

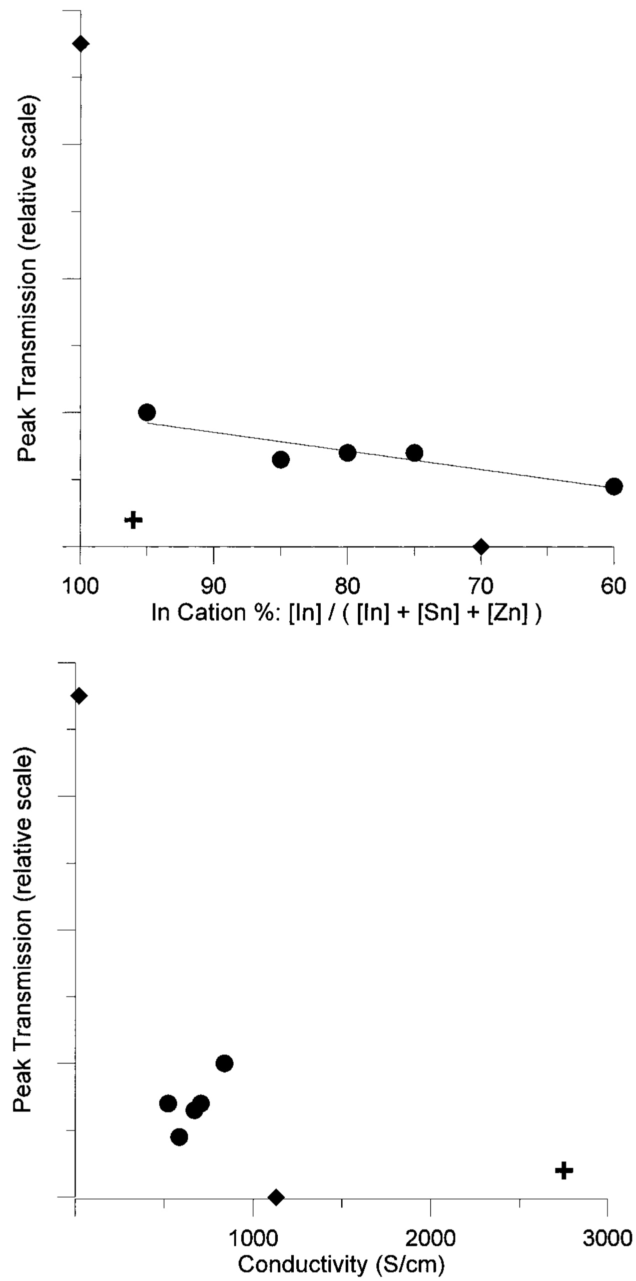

Figure 5. Plot of peak (500 nm) transmittance versus cation % In (a, top) and versus conductivity (b, bottom). Samples shown are (◆) cosubstituted copper-quenched including pure In$_2$O$_3$, (●) air-quenched cosubstituted, (+) 4 cation % Sn ITO.

Figure 5 shows the dependence of peak (500 nm) transmission on conductivity and cosubstitution. All samples show significantly lower peak transmissions than in pure In$_2$O$_3$. The lowest value was observed in the 70 cation % In copper-quenched sample, which combined high conductivity with large extent of cosubstitution. The highest transmission (other than in pure In$_2$O$_3$) was from the relatively lightly cosubstituted 95 cation % In sample. There is a strong correlation between higher conductivity and lower transmission. A weak correlation exists between cosubstitution extent and lower transmission. These trends are supported by the observed sample colors. Samples with lower peak transmissions were visually darker (see Table 2).

(28) Aldrich Chemical Co., Catalog Numbers 26408-3, 26565-9, and 26636-1, 1994.

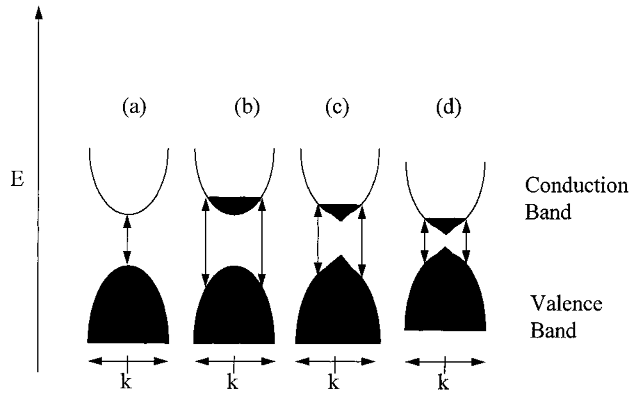

Figure 6. Schematic band structure diagram for cosubstituted In_2O_3. (a) The direct bandgap of an undoped semiconductor, e.g., pure In_2O_3. (b) In degenerate doped semiconductors such as ITO, the filling of states causes the direct bandgap to increase (Moss−Burstein shift). (c) Many-body effects in ITO cause a partial bandgap narrowing but the overall bandgap is still larger than in In_2O_3. (d) Creation of acceptor−donor pairs in cosubstituted In_2O_3 causes a dramatic bandgap narrowing effect which often makes the overall bandgap smaller than in pure In_2O_3.

Application. $In_{2-2x}Sn_xZn_xO_{3-\delta}$ ($x = 0-0.4$) is a TCO with significantly less indium than bulk ITO. The costs of Zn and Sn are roughly 1% and 40% that of In, respectively, at the present moment.[28] Although cosubstitution causes a gradual lowering of bulk conductivity and transparency, the economic benefits of reduced In content make $In_{2-2x}Sn_xZn_xO_{3-\delta}$ interesting for commercial investigation. Thin-film studies of $In_{2-2x}Sn_xZn_xO_{3-\delta}$ are needed to compare phase behavior and defect chemistry.

Conclusion

The solid solubility of ZnO, SnO_2, and ZnO/SnO_2 in bulk In_2O_3 has been studied using powder X-ray diffraction. Cosubstitution of ZnO and SnO_2 creates a net isovalent substitution that increases the solid solubility from 6 cation % Sn in ITO and approximately 0 cation % in Zn-doped In_2O_3 to 40 cation % Zn and Sn (combined) in $In_{1.2}Sn_{0.4}Zn_{0.4}O_3$. The cubic bixbyite structure is retained as the lattice parameter contracts from 10.120 to 9.994 Å. Cosubstituted In_2O_3 shows conductivities varying from 500 to 2500 S/cm. Optimum conductivites are achieved by limiting the extent of cosubstitution and by rapid quenching. In addition, limited cosubstitution correlates with higher peak transparency and wider optical bandgap. However, the high cost of In metal makes relevant the study of more extensively cosubstituted In_2O_3. In addition, learning the effects of multiple substituents in known TCOs is a first step toward rational design of new multication TCOs.

Acknowledgment. This work was supported by the MRSEC program of the National Science Foundation (DMR-9632472) at Northwestern University and made use of the Central Facilities of the same MRSEC program. George Palmer was supported by a National Defense Science and Engineering Graduate fellowship funded by the Office of Naval Research. Dr. Jon Schindler and Professor Carl Kannewurf of the Electrical and Computer Engineering Department at Northwestern University provided training on and use of the four-probe conductivity apparatus. Doreen Edwards of the Department of Materials Science and Engineering at Northwestern University provided helpful conversation and insights.

CM9704037